Accounting for Fiber Bending Effects in Homogenization of Long Fiber Reinforced Composites

Poulios, Konstantinos; Niordson, Christian Frithiof

Published in:
Proceedings of the 20th International Conference on Composite Materials

Publication date:
2015

Document Version
Peer reviewed version

ACCOUNTING FOR FIBER BENDING EFFECTS IN HOMOGENIZATION OF LONG FIBER REINFORCED COMPOSITES

Konstantinos Poulios[1], Christian F. Niordson[2]
Department of Mechanical Engineering, Technical University of Denmark
Nils Koppels Allé, Building 403, DK-2800 Kgs. Lyngby, Denmark
[1]Email: kopo@mek.dtu.dk [2]Email: cn@mek.dtu.dk

Keywords: Homogenization, Fiber bending stiffness, Finite-element

ABSTRACT

The present work deals with homogenized finite-element models of long fiber reinforced composite materials in the context of studying compressive failure modes such as the formation of kink bands and fiber micro-buckling. Compared to finite-element models with an explicit discretization of the material micro-structure including individual fibers, homogenized models are computationally more efficient and hence more suitable for modeling of larger and complex structure. Nevertheless, the formulation of homogenized models is more complicated, especially if the bending stiffness of the reinforcing fibers is to be taken into account. In that case, so-called higher order strain terms need to be considered. In this paper, important relevant works from the literature are discussed and numerical results from a new homogenization model are presented. The new model accounts for two independent constitutive laws for the fiber and the matrix materials, respectively expressed in the frameworks of hyper-elasticity and hyper-elasto-plasticity. The presented numerical results include comparisons between the homogenized model and an explicit discretization of the composite micro-structure. Both models are in good agreement. In cases where the fiber bending stiffness is significant, the homogenized finite-element model exhibits size-scale dependent material behavior, as predicted by the model with explicitly discretized individual fibers.

1 INTRODUCTION

Compared to homogeneous materials of the same weight or price, long fiber reinforced composites normally offer superior mechanical strength with the exception of compressive loading. Failure modes under compression include the formation of kink bands, fiber micro-buckling and debonding, which have all been extensively studied both experimentally and numerically. For instance in [1], Kyriakides et al. address the compressive failure of long fiber reinforced composites both presenting experimental and numerical results. The latter are based on a finite-element model with an explicitly discretized material micro-structure. The experimental part in [1], was not limited to the demonstration of a compressive failure mechanism and the evaluation of effective material properties for a fiber reinforced composite material. It also assessed fiber alignment imperfections in the tested samples quantitatively and determined material properties of the individual constituents. Both the fiber misalignment data and the constituent properties were important input for the theoretical part of the paper. In total, the results presented in [1] confirmed the impact of fiber imperfections on the compressive limit load of the tested composite and demonstrated both experimentally and theoretically, that inclined kink bands of a rather reproducible width start to form directly after the limit load.

In [2], Fleck & Shu provided an exclusively theoretical study. They introduced a homogenized finite-element model capable of capturing the fiber bending stiffness and they presented a series of practical numerical examples based on that model. The main characteristic of their model is the internal kinematic variable θ, which represents a micro-rotation of the fibers. Based on the two components of the homogenized displacement field u and the additional variable θ, a 2D finite-element model with three unknowns per node was formulated. A higher-order stress (couple stress), work conjugate to the angle θ was identified and the equivalence of the derived formulation with the Cosserat theory was demonstrated. With regard to the provided numerical results a set of examples was studied, with a fiber waviness imperfection running through the complete sample height, similar

to the examples studied in [1]. In a second set of examples the assumed fiber imperfection was limited in an elliptical region at the center of the sample and the impact of the size of this elliptical region on the critical load was investigated.

Plasticity in [2] was modeled through a Ramberg-Osgood constitutive law, expressed in terms of effective stress and strain measures for the composite. A different approach regarding the modeling of plasticity was followed in [3], where Christoffersen & Jensen provided a homogenized finite-element formulation, which was based on two independent material laws for the two constituents of long fiber reinforced composites. This is a micro-mechanical description of the composite material, compared to the rather phenomenological plasticity model utilized in [2]. Nevertheless, the model presented in [3] does not account for the bending stiffness of the reinforcing fibers.

The numerical results presented in this paper are obtained with two different models, one with an explicit discretization of individual fibers, as in [1] and [4], and a homogenized model which combines the advantages of [2] and [3]. The role of the individual fiber model is to serve as a reference for the homogenized one.

2 HOMOGENIZED MODEL

This section provides some basic information regarding the homogenized finite-element model considered in this paper. Similar to [2], this new model, relies on additional internal kinematic variables for describing the deformation state of the material micro-structure. In contrast to [2] however, which requires only an one-dimensional internal kinematic variable θ, corresponding to the rotation of the fiber cross section at the micro-level, our model relies on a two-dimensional internal kinematic variable d_B, which captures possible deviations between the deformation states of the fiber and the matrix in a more generic way. Fig. 1 illustrates the impact of each component of d_B on the deformation state of the material micro-structure.

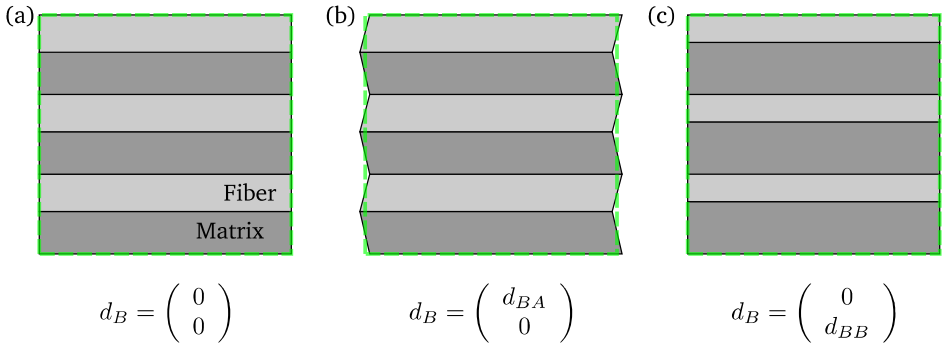

Figure 1: Deformation states of the composite micro-structure corresponding to different values of the internal kinematic variable d_B.

Adding the degrees of freedom of the internal kinematic variable d_B to the two degrees of freedom of the homogenized displacement variable u, our homogenized finite-element model requires four kinematic degrees of freedom per node, instead of three nodal degrees of freedom considered in [2]. In addition, a plastic multiplier variable γ_m describing isotropic hardening of the matrix material is also considered as an unknown, resulting a total of five nodal degrees of freedom. The cost of the additional two variables is compensated by the greater flexibility and generality of our formulation as well as by its stricter micro-mechanical foundation.

A detailed description of this homogenized model can be found in [5]. Its basic characteristic is that two independent deformation gradients are defined for the matrix and the fiber materials respectively, through closed form expressions in terms of the kinematic variables u and d_B:

$$F_m = I + \nabla u + \frac{1}{c_m} d_B N_B^T \tag{1}$$

$$F_f = I + \nabla u - \frac{1}{c_f} d_B N_B^T \tag{2}$$

In these expressions, c_m and c_f are the volume fraction ratios of the matrix and the fiber materials respectively, with $c_m + c_f = 1$. The unit vector N_B corresponds to the direction perpendicular to the reinforcing fibers in the undeformed configuration.

In order to account for the bending stiffness of the fibers, an enhanced version of F_f is defined as a function of the signed distance χ_B from the fiber middle line:

$$\widetilde{F}_f(\chi_B) = F_f - \chi_B \frac{1}{c_f} \nabla d_B N_A N_A^T \tag{3}$$

where N_A is the unit vector representing the direction parallel to the fibers in the undeformed configuration.

With the deformation gradients in each constituent given by expressions (1) and (3), force equilibrium and plastic deformation can be modeled in the frameworks of hyper-elasticity and hyper-elasto-plasticity for the fiber and the matrix phases respectively. In hyper-elastic material models, with or without plastic deformation, the material response is described by a free energy density function in terms of a frame indifferent measure of the corresponding deformation gradient, like e.g. the left Cauchy-Green tensor, defined as $F F^T$. Such free energy functions can be written for the two constituents as:

$$\psi_m = \psi_m(F_m^e F_m^{e\,T}) = \psi_m(\nabla u, d_B, \gamma_m) \tag{4}$$

$$\psi_f = \psi_f(\widetilde{F}_f \widetilde{F}_f^T) = \psi_f(\nabla u, d_B, \chi_B \nabla d_B) \tag{5}$$

In expression (4), F_m^e is the elastic part of F_m, defined through the usual multiplicative decomposition of the deformation gradient. For more details on the multiplicative split in the context of hyper-elasto-plasticity, the reader is referred to [5] or [6]. In contrast to the matrix phase, the fiber material is assumed to remain in the elastic regime. The total virtual work desnsity for the composite material can be written, based on (4) and (5), as:

$$\delta\psi = c_m \delta\psi_m + c_f \frac{1}{h_f} \int_{-h_f/2}^{h_f/2} \delta\psi_f \, d\chi_B = \delta\psi(\nabla \delta u, \delta d_B, \nabla \delta d_B, \delta\gamma_m) \tag{6}$$

Note that in expression (6), χ_B is eliminated by performing an analytical integration through the fiber height h_f.

Force equilibrium is expressed by the equality between the internal virtual work from (6) and the virtual work of external forces at the boundary and the volume of the considered body. Imposing this equality for variations δu and δd_B defined through the basis functions of the corresponding finite-element approximations, provides a sufficient number of equations for solving for the unknowns u and d_B. An additional equation is required for solving also for the plastic multiplier γ_m. This remaining equation is the plasticity consistency condition:

$$Y_m(\gamma_m) = \sqrt{\frac{3}{2}} \|\sigma_m(\nabla u, d_B, \gamma_m)\| \tag{6}$$

where Y_m is the matrix material yield limit (including hardening) and σ_m is the Cauchy stress in the matrix material. Eq. (6) is imposed inside the plastic zone in a weighted residual sense, with the weighting functions $\delta\gamma_m$ corresponding to the basis functions of the finite-element approximation of the plastic multiplier. Outside the plastic zone the condition $\gamma_m = \gamma_{m0}$ is imposed also in a weighted residual sense, with γ_{m0} standing for the plastic multiplier value at the previous time step.

3 NUMERICAL RESULTS

Fig. 2 shows a square sample of a fiber reinforced composite material, with the reinforcing fibers nominally aligned in the horizontal direction. The sample is fixed at its left side, while its right side is free to move as a rigid body in the vertical direction while its horizontal displacement is prescribed, e.g. through a double acting hydraulic cylinder. The fiber height h_f is equal to 0.015 mm and there are 40 fibers, evenly distributed along the sample height. These data combined with the sample height of 1 mm result in a fiber content c_f equal to 0.6. The considered sample includes a prescribed sinusoidal waviness imperfection of the fibers with amplitude of 0.01 mm and half-period equal to the sample length of 1 mm, which is constant through the sample height.

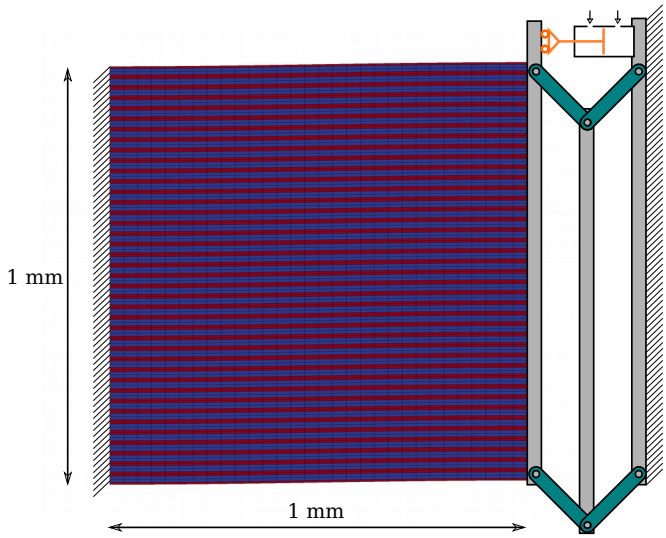

Figure 2: Fiber reinforced composite sample with 40 fibers and $c_f = 0.6$ and boundary conditions.

The Young's modulus of the reinforcing fibers is $E_f = 3.5$ GPa and their Poisson's ratio is $\nu_f = 0.263$, while the matrix material has a Young's modulus $E_m = 0.1$ GPa, a Poisson's ratio $\nu_m = 0.356$ and a Ramberg-Osgood hardening behavior with initial yield stress $\sigma_{ym} = 0.013 E_m$, yield offset $\alpha_m = 3/7$ and hardening exponent $n_m = 4$. All data for this example are taken from the main example presented in [4].

3.1 Results from the model with an explicit discretization of individual fibers

The mesh of the individual fiber model, shown in Fig. 2, consists of 30 elements along the length of the sample, 2 elements along the height of each fiber layer and 2 elements along the height of each matrix layer. The displacement unknown u is defined in both the matrix and the fiber elements, while a plastic multiplier unknown γ_m is defined only in the matrix elements. Both u and γ_m are approximated with eight-node quadrilateral elements.

Fig. 3 shows deformation states of the considered sample at different values of the prescribed horizontal compression. The left picture corresponds to the limit load at buckling initiation, equal to 25.88 kN, while the right pictures corresponds to a nominal compression of 2%. The color scale corresponds to the increase of the plastic multiplier γ_m in the matrix material during the current step.

Fig. 4 shows equivalent results for an increased number of 80 fiber along the sample height. The fiber height is reduced accordingly to 0.0075 mm in order to preserve the initial fiber content of 0.6. The limit load corresponding to the left picture of Fig. 4 is 25.5 kN. Compared to Fig. 3, the deformation presented in the right picture of Fig. 4 for a compression of 2% exhibits a considerably sharper bending radius at the beginning of the observed kink band.

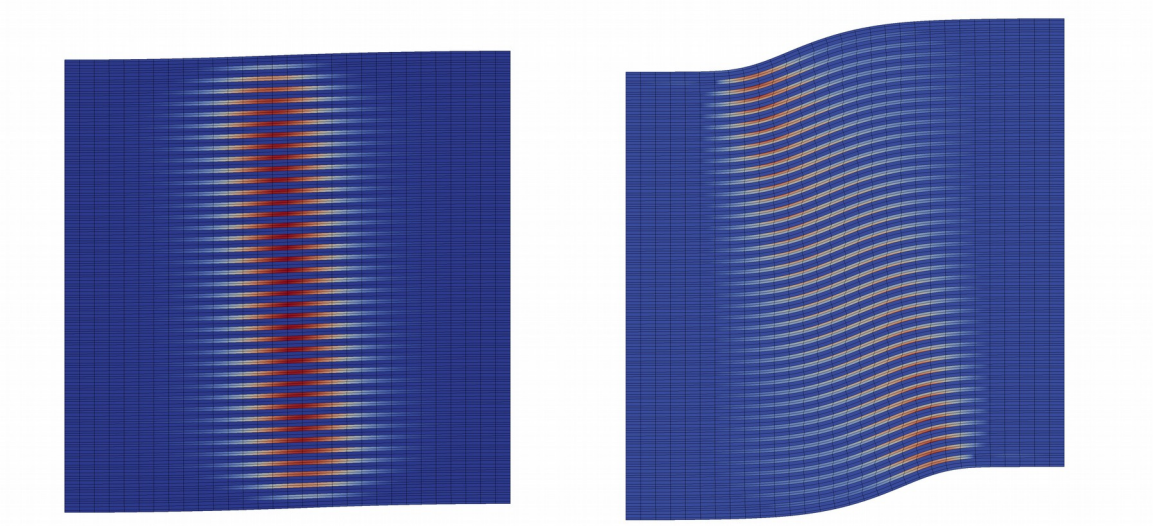

Figure 3: Deformation states of the composite material sample with 40 fibers at the limit load (left) and at a nominal compression of 2% (right) for an explicit discretization of individual fibers.

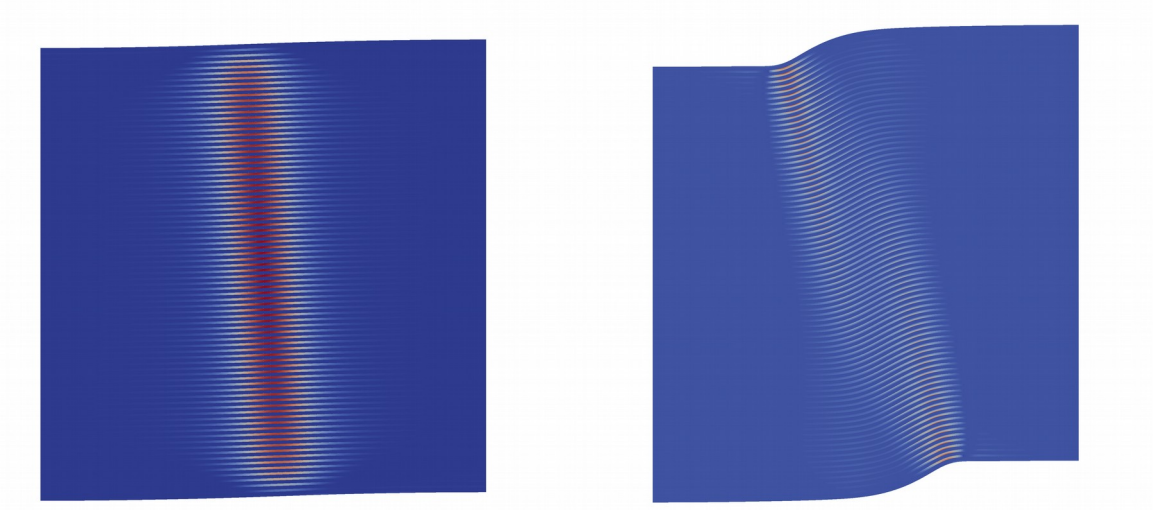

Figure 4: Deformation states of the composite material sample with 80 fibers at the limit load (left) and at a nominal compression of 2% (right) for an explicit discretization of individual fibers.

3.2 Results from the homogenized model

In the homogenized model there is no distinction between matrix and fiber elements. The whole structure is discretized by 20 times 20 elements in the horizontal and vertical directions respectively. All three unknowns u, d_B and γ_m are discretized with eight-node quadrilateral elements. The results shown in Figs. 5 and 6 are equivalent to the results of Figs. 3 and 4 respectively. It appears that the homogenized model can capture the shape and the extent of the zone where plastic deformation in the matrix materials takes place, both close to the buckling initiation as well as in the post-buckling phase. Moreover the homogenized model captures the different bending radius at the beginning of the kink band, as it was also observed in the results from the individual fiber model. The limit loads corresponding to the left pictures of Figs. 5 and 6 are 27.0 and 26.6 kN respectively. These values are approximately 4% higher than the corresponding limit loads from section 3.1.

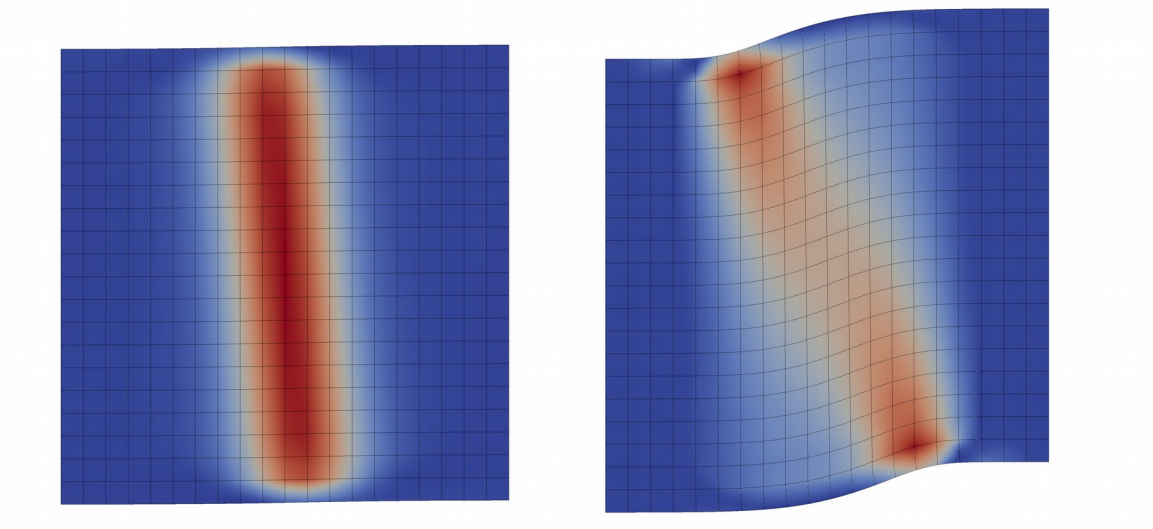

Figure 5: Deformation states of the composite material sample with 40 fiber at the limit load (left) and at a nominal compression of 2% (right) for the homogenized model.

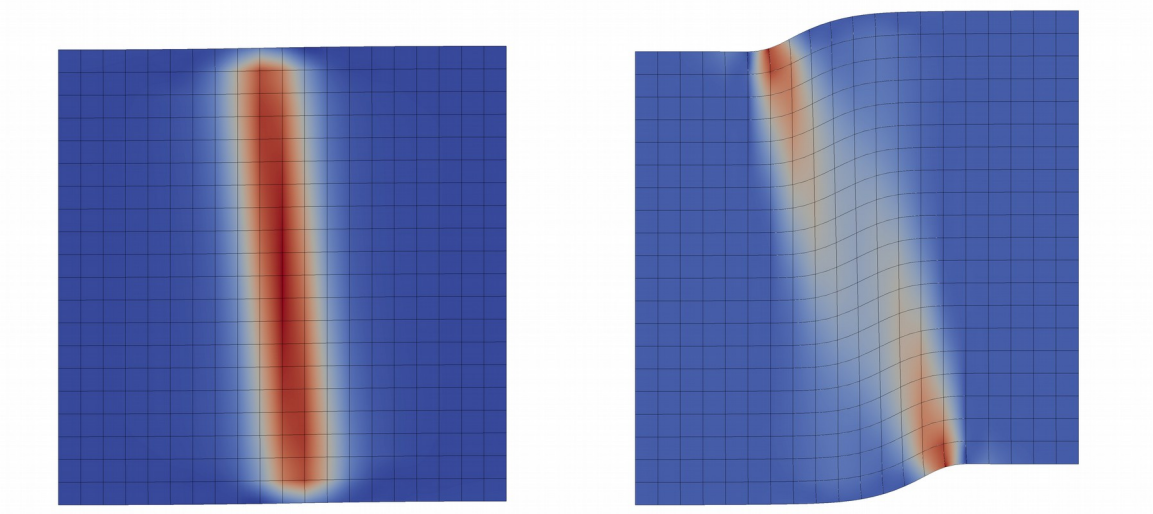

Figure 6: Deformation states of the composite material sample with 80 fiber at the limit load (left) and at a nominal compression of 2% (right) for the homogenized model.

3.3 Comparison

A preliminary comparison of the results presented in subsections 3.1 and 3.2 shows a good agreement between the homogenized and the reference model. This section includes some additional results for assessing the validity of the homogenized model. Figs. 7 and 8 show the axial force versus compression responses calculated for 40 and 80 fibers based on the reference and the homogenized model, respectively. Apart from the slightly higher buckling initiation load predicted by the homogenized model, which has already been mentioned, comparison of the diagrams in Figs. 7 and 8 shows that the homogenized model captures the impact of the fiber diameter on the post-buckling response very accurately.

The incremental values of γ_m presented in Figs. 3 to 6 show a good agreement between the two models with respect to the shape of the plastic zone and the intensity of the plastic flow. Nevertheless, these incremental quantities depend on the the load step size and their magnitudes are not directly comparable in a variable load step simulation. More appropriate for a quantitative comparison is the the cumulative value of γ_m. Figs. 9 and 10 provide a comparison of the two models with regard to

the evolution of the plastic multiplier γ_m at the center of the sample as a function of the applied nominal compression. The slightly shifted buckling point is visible also in these comparisons, but otherwise there is a very good agreement between the two models both for the case with 40 fibers as well as for the case with 80 fibers.

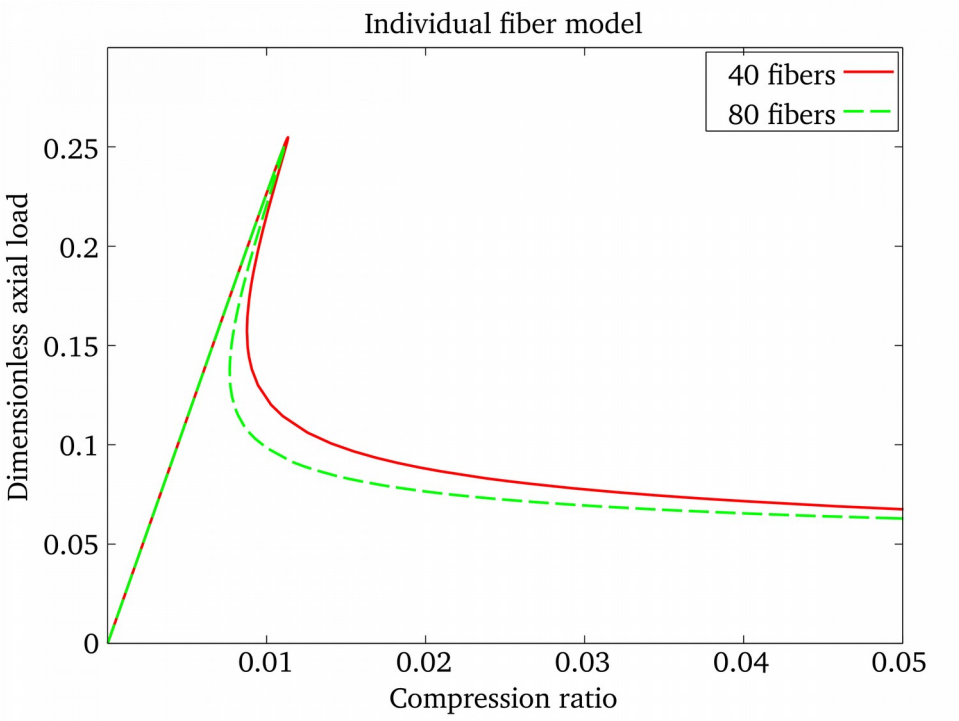

Figure 7: Axial force versus compression response from the individual fiber model.

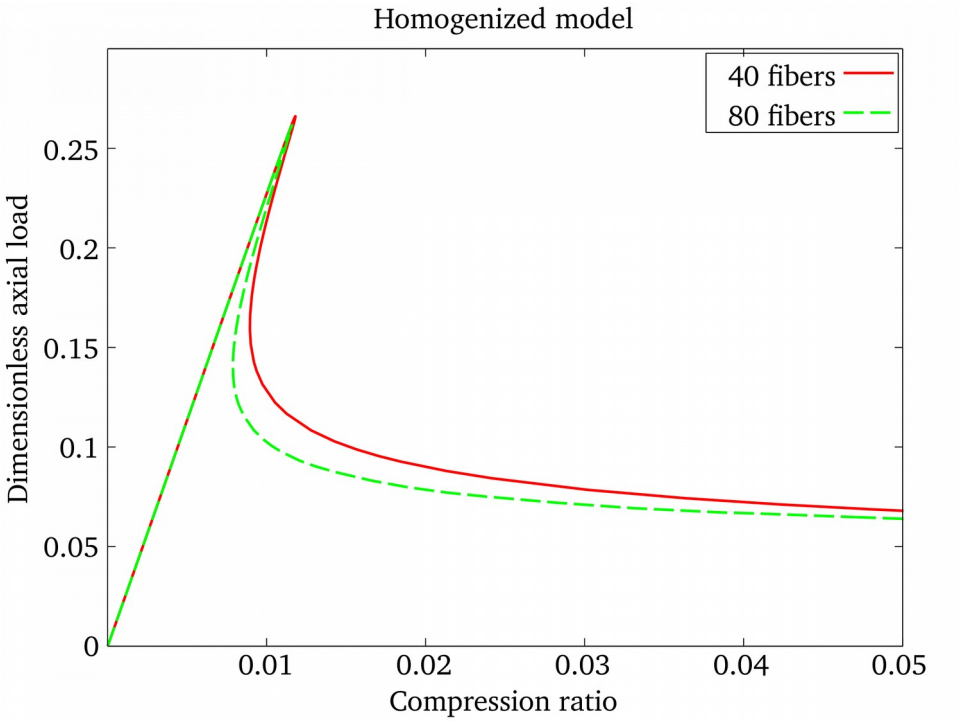

Figure 8: Axial force versus compression response from the homogenized model.

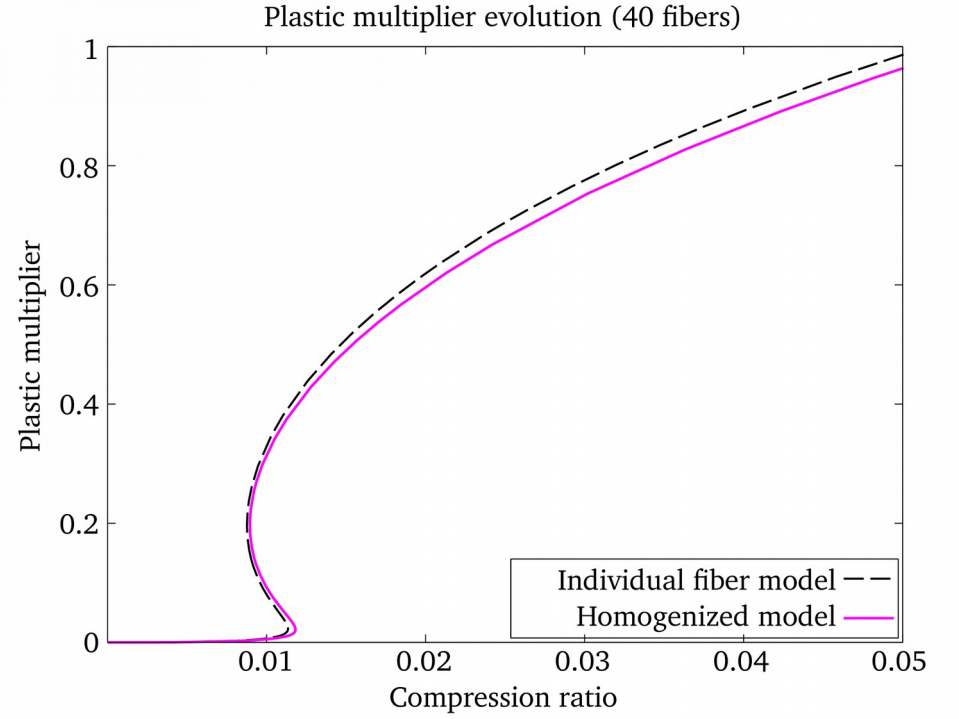

Figure 9: Evolution of the plastic multiplier in the matrix material at the center of the fiber composite sample with 40 fibers.

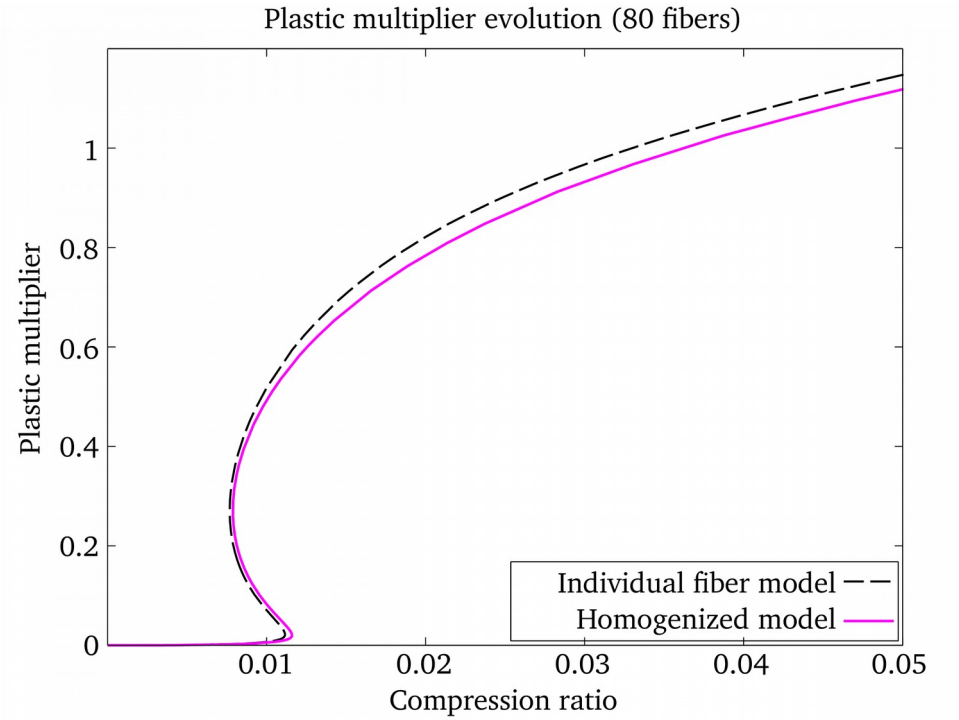

Figure 10: Evolution of the plastic multiplier in the matrix material at the center of the fiber composite sample with 80 fibers.

4 CONCLUSIONS

The numerical results presented in this work demonstrated the capabilities and the level of accuracy of a homogenized model for long fiber reinforced composite materials, compared to an equivalent model with an explicit discretization of individual fibers. The comparison between the two models revealed a generally good agreement. More specifically, the homogenized model was capable of simulating the formation of a kink band during the compression of a fiber reinforced composite sample, including the impact of the fiber diameter on the initiation and evolution of the observed kink band. The deviation between the two models with regard to the buckling initiation load was limited to 4%. Moreover, this deviation was not related to the fiber bending stiffness, as it was the same for both fiber diameters that were studied.

ACKNOWLEDGEMENTS

This work was supported by the Danish Council for Independent Research, through the Sapere Aude project “Higher Order Theories in Solid Mechanics”.

REFERENCES

[1] S. Kyriakides, R. Arseculeratne, E. J.Perry, and K. M. Liechti, On the compressive failure of fiber reinforced composites, *International Journal of Solids and Structures*, **32** (6-7), 1995, pp. 689-738.

[2] N. A. Fleck and J. Y. Shu, Microbuckle initiation in fibre composites: A finite element study, *Journal of the Mechanics and Physics of Solids*, **43(**12), 1995, pp. 1887-1918.

[3] J. Christoffersen and H. M. Jensen, Kink band analysis accounting for the microstructure of fiber reinforced materials, *Mechanics of Materials*, **24** (4), 1996, pp. 305-315.

[4] J. L. Wind, S. Steffensen, and H. M. Jensen, Comparison of a composite model and an individually fiber and matrix discretized model for kink band formation, *International Journal of Non-linear Mechanics*, **67**, 2014, pp. 319-325.

[5] K. Poulios, C. F. Niordson, Homogenization of long fiber reinforced composites including fiber bending effects, (submitted).

[6] J. Simo, Algorithms for static and dynamic multiplicative plasticity that preserve the classical return mapping schemes of the infinitesimal theory, *Computer Methods in Applied Mechanics and Engineering*, **99** (1), 1992, pp. 61-112.